

The dynamical and thermodynamic effects of turbulence for the cosmic baryonic fluid

YUN WANG (王云),¹ MINXING LI (李敏行),¹ AND PING HE (何平)^{1,2}

¹*College of Physics, Jilin University, Changchun 130012, China.*

²*Center for High Energy Physics, Peking University, Beijing 100871, China.*

ABSTRACT

Both simulations and observations indicate that the so-called missing baryons reside in the intergalactic medium (IGM) known as the warm-hot intergalactic medium (WHIM). In this article, we demonstrate that turbulence in the cosmic baryonic fluid is crucial for correctly understanding both the spatial distribution and the physical origins of the missing baryons in the universe. First, we find that dynamical effects cause the gas to be detained in low-density and intermediate-density regions, resulting in high baryon fractions, while prevent the inflow of the gas in high-density regions, leading to low baryon fractions. Second, turbulent energy is converted into thermal energy, and the injection and dissipation of turbulent energy have essentially reached a balance from $z = 1$ to 0. This indicates that the cosmic fluid is in a state of fully-developed turbulence within this redshift range. Due to turbulent heating, as redshift decreases, an increasing amount of warm gas is heated and transitions into the WHIM, and some even into hot gas.

Keywords: Intracluster medium (858); Large-scale structure of the universe (902); Wavelet analysis (1918); Astrophysical fluid dynamics (101); Hydrodynamical simulations (767)

1. INTRODUCTION

According to the standard cosmological model, approximately 5% of the total energy density of the universe consists of baryonic matter, which includes protons and neutrons. However, observations of stars, galaxies, and the surrounding gas have shown that about 30% – 40% of the predicted baryons are missing (Fukugita et al. 1998; Bregman 2007; Fang 2018). Scientists speculate that these missing baryons may reside in a low-density high-temperature plasma, known as the WHIM (Cen & Ostriker 1999; Davé et al. 2001; Fang et al. 2002, 2006; Branchini et al. 2009).

In recent years, with the advancement of new astronomical observation techniques and methods, scientists have been able to detect some of the previously undetectable baryons through X-ray and radio facilities (Nicastro et al. 2018; Nevalainen et al. 2019; Macquart et al. 2020). These studies support the idea that these baryons in the universe are not truly missing but are present in the IGM within the cosmic web structures. Despite significant progress, the precise locations and physical origins of the missing baryons remain elusive (Driver 2021).

Based on our previous series of works (Kim et al. 2005; He et al. 2006; Yang et al. 2020, 2022; Wang & He 2024a,b), in this work, we demonstrate that turbulence in the cosmic baryonic fluid is crucial for correctly understanding both the spatial distribution and the physical origins of the missing baryons in the universe. The consensus reached is that turbulence can occur at any scale in the cosmic fluid, which has been extensively studied both theoretically (Norman & Bryan 1999; Brüggén et al. 2005; Cassano & Brunetti 2005; Dolag et al. 2005; Subramanian et al. 2006; Roediger & Brüggén 2007; Ryu et al. 2008; Lau et al. 2009; Zhu et al. 2010; Gaspari et al. 2011; Evoli & Ferrara 2011; Vazza et al. 2012; Zhu et al. 2013; Banerjee & Sharma 2014; Miniati 2014; Porter et al. 2015; Iapichino et al. 2017; Angelinelli et al. 2020) and observationally (Vogt & Enßlin 2003; Schuecker et al. 2004; Murgia et al. 2004; Enßlin & Vogt 2006; Bonafede et al. 2010; Vacca et al. 2010; Churazov et al. 2012; Zhuravleva et al. 2014; Walker et al. 2015; Khatri & Gaspari 2016; Shi & Zhang 2019). Through dynamical and thermodynamic investigations, we provide a detailed analysis of how turbulence influences the distribution of baryonic matter in cosmic space and offer a theoretical explanation for the missing baryon problem.

The paper is organized as follows. In Section 2, we briefly introduce our methods used in this work. In Section 3, we present the results of our work. In Section 4, we present the conclusions and discussions of the paper.

2. METHODS

We divide the space into the following regions, according to the dark matter density $\Delta_{\text{dm}}(\mathbf{x}) = \rho_{\text{dm}}(\mathbf{x})/\bar{\rho}_{\text{dm}}$, as (1) low-density, with $\Delta_{\text{dm}}(\mathbf{x}) < 0.2 - 0.5$, depending on redshifts, (2) intermediate-density, with $0.2 - 0.5 < \Delta_{\text{dm}}(\mathbf{x}) < 200$, (3) high-density, with $200 < \Delta_{\text{dm}}(\mathbf{x}) < 10^3$, and (4) extremely high-density, with $\Delta_{\text{dm}}(\mathbf{x}) > 10^3$, which roughly correspond to (1) voids and under-dense regions, (2) filaments, sheets and outskirts of clusters on the cosmic web, (3) virialized structures such as galaxy clusters, and (4) galaxies in clusters. This classification scheme is roughly consistent with that of Vazza et al. (2009).

Similar to Bregman (2007), we also define 4 components of baryonic matter, as (1) hot gas, with $T > 10^7\text{K}$, (2) WHIM, with $10^5\text{K} < T < 10^7\text{K}$, (3) warm gas, with $T < 10^5\text{K}$, and (4) cold component, with star, AGN (black hole) and (possible) others.

2.1. Divergence of velocity field and dynamical effects

For the velocity field \mathbf{u} of the cosmic fluid, the dynamical equation of its divergence $d = \nabla \cdot \mathbf{u}$, or the compression rate, is as follows (Zhu et al. 2010, 2011; Schmidt et al. 2017):

$$\frac{Dd}{Dt} \equiv \frac{\partial d}{\partial t} + \frac{1}{a} \mathbf{u} \cdot \nabla d = Q_{\text{turb}} + Q_{\text{th}} + Q_{\text{grav}} + Q_{\text{exp}}, \quad (1)$$

with

$$\begin{aligned} Q_{\text{turb}} &= \frac{1}{a} \left(\frac{1}{2} \omega^2 - S_{ij}^2 \right), \\ Q_{\text{th}} &= \frac{1}{a} \left(\frac{1}{\rho_b^2} \nabla \rho_b \cdot \nabla P - \frac{1}{\rho_b} \nabla^2 P \right), \\ Q_{\text{grav}} &= -\frac{4\pi G}{a^2} (\rho_{\text{tot}} - \bar{\rho}_0), \\ Q_{\text{exp}} &= -\frac{\dot{a}}{a} d, \end{aligned} \quad (2)$$

in which a is the scale factor, and the thermal pressure P can be computed using equation (10). Q_{turb} , Q_{th} , Q_{grav} and Q_{exp} indicate the dynamical effects of turbulence, thermal, gravitational collapse, and cosmic expansion, respectively, and $Q_{\text{tot}} = Q_{\text{turb}} + Q_{\text{th}} + Q_{\text{grav}} + Q_{\text{exp}}$ represents their total combined effects. In the above expression, $\boldsymbol{\omega} \equiv \nabla \times \mathbf{u}$ represents the vorticity, and $S_{ij} \equiv (1/2)(\partial_i u_j + \partial_j u_i)$ represents the strain rate of the velocity field for the cosmic fluid.

2.2. Mass fraction and baryon fraction

For the simulation data, we define the total mass fraction within the simulation volume as a function of redshift as

$$f_{\mathbf{x}}(z) = \frac{M_{\mathbf{x}}(z)}{M_{\text{total}}}, \quad (3)$$

where the subscript ‘x’ refers to the 4 baryonic components, $M_{\mathbf{x}}(z)$ denotes the total mass of the x-component at redshift

z , and M_{total} refers to the total baryonic mass within the simulation box.

We specifically designate a sequence of dark matter densities as follows:

$$0 = \delta_0 < \delta_1 < \dots < \delta_i < \dots < \delta_N = \infty, \quad (4)$$

and hence, the i -th density interval is

$$\delta_{i-1} < \Delta_i < \delta_i, \quad i = 1, 2, \dots, N, \quad (5)$$

where N is a sufficiently large number.

For the spatial points within the i -th dark matter density interval at redshift z , we count the masses of the 4 baryonic components defined earlier, as $m_{\mathbf{x}}(\Delta_i, z)$, and we define the cumulative mass fraction of the 4 baryonic components that depend on dark matter density as

$$F_{\mathbf{x}}(\Delta_i, z) = \frac{1}{M_{\text{total}}} \sum_{k=N}^i m_{\mathbf{x}}(\Delta_k, z), \quad 1 \leq i \leq N. \quad (6)$$

Note that the summation in the above expression is performed in descending order from N to i , that is, from high-density to low-density regions. The total cumulative mass fraction is defined by summation over the 4 baryonic components as

$$F_{\text{tot}}(\Delta_i, z) = \sum_{\mathbf{x}=1}^4 F_{\mathbf{x}}(\Delta_i, z). \quad (7)$$

We also need to define baryon fraction as a function of spatial positions and redshift for our work, as

$$f_{\text{b}}(\mathbf{x}, z) = \frac{\rho_{\text{b}}(\mathbf{x}, z)}{\rho_{\text{dm}}(\mathbf{x}, z) + \rho_{\text{b}}(\mathbf{x}, z)}, \quad (8)$$

where $\rho_{\text{b}}(\mathbf{x}, z)$ and $\rho_{\text{dm}}(\mathbf{x}, z)$ are the baryonic matter and dark matter density, respectively.

2.3. Turbulent and thermal energy of the baryonic field

TNG provides the internal energy per unit mass of baryonic gas, $e_{\text{u}}(\mathbf{x})$. Hence we have the thermal energy density,

$$\varepsilon_{\text{th}}(\mathbf{x}) = \rho_{\text{b}}(\mathbf{x}) e_{\text{u}}(\mathbf{x}) = \frac{3}{2} \frac{\rho_{\text{b}}(\mathbf{x})}{\mu(\mathbf{x}) m_{\text{p}}} k_{\text{B}} T(\mathbf{x}), \quad (9)$$

where k_{B} is the Boltzmann constant, and m_{p} the mass of the proton. $\mu(\mathbf{x})$, $\rho_{\text{b}}(\mathbf{x})$ and $T(\mathbf{x})$, dependent on the spatial locations, are the mean molecular weight, mass density, and temperature of the baryonic fluid, respectively. Regarding the cosmic fluid as the monoatomic ideal gas, its thermal pressure is

$$P(\mathbf{x}) = \frac{\rho_{\text{b}}(\mathbf{x})}{\mu(\mathbf{x}) m_{\text{p}}} k_{\text{B}} T(\mathbf{x}) = \frac{2}{3} \varepsilon_{\text{th}}(\mathbf{x}). \quad (10)$$

The turbulent energy density is

$$\varepsilon_{\text{turb}} = \frac{1}{2} \rho_b(\mathbf{x}) \mathbf{u}_{\text{turb}}^2(\mathbf{x}), \quad (11)$$

in which $\mathbf{u}_{\text{turb}}(\mathbf{x})$ is the three-dimensional velocity of turbulent flow. In general, a velocity field of the fluid \mathbf{u} is a superposition of the turbulent velocity and the bulk velocity, i.e. $\mathbf{u} = \mathbf{u}_{\text{turb}} + \mathbf{u}_{\text{bulk}}$. As in Wang & He (2024a,b), we also use the iterative multi-scale filtering approach developed by Vazza et al. (2012) to extract turbulent motions from the velocity field of the cosmic fluid.

We also define the ratio of turbulent energy to thermal energy as

$$r(\mathbf{x}) \equiv \frac{\varepsilon_{\text{turb}}(\mathbf{x})}{\varepsilon_{\text{th}}(\mathbf{x})} = \frac{\mathbf{u}_{\text{turb}}^2(\mathbf{x})}{2e_u(\mathbf{x})}. \quad (12)$$

For the random velocity field of the cosmic baryonic fluid $\mathbf{u}_{\text{turb}}(\mathbf{x})$ with the zero mean value, its isotropic continuous wavelet transform (CWT) $\tilde{\mathbf{u}}_{\text{turb}}(w, \mathbf{x})$ is obtained by convolution with the wavelet function Ψ as

$$\tilde{\mathbf{u}}_{\text{turb}}(w, \mathbf{x}) = \int \mathbf{u}_{\text{turb}}(\boldsymbol{\tau}) \Psi(w, \mathbf{x} - \boldsymbol{\tau}) d^3\boldsymbol{\tau}. \quad (13)$$

Throughout this work, we use the so-called 3D isotropic cosine-weighted Gaussian-derived wavelet (CW-GDW), which can achieve good localization in both spatial and frequency space simultaneously (Wang & He 2022, 2024c,a). With $\tilde{\mathbf{u}}_{\text{turb}}(w, \mathbf{x})$, and referring to equation (11), we define the local wavelet power spectrum (WPS) for the turbulent velocity $\tilde{\mathbf{u}}_{\text{turb}}(w, \mathbf{x})$ as

$$S_{\text{turb}}(w, \mathbf{x}) \equiv \frac{1}{2} \Delta_b(\mathbf{x}) |\tilde{\mathbf{u}}_{\text{turb}}(w, \mathbf{x})|^2. \quad (14)$$

Note that here we do not use $\rho_b(\mathbf{x})$ directly, but instead use $\Delta_b(\mathbf{x}) = \rho_b(\mathbf{x})/\bar{\rho}_b$ for the calculations, where $\bar{\rho}_b$ is the background baryonic density.

Then we define the environment-dependent WPS as

$$S_{\text{turb}}(w, \delta) \equiv \frac{1}{2} \langle \Delta_b(\mathbf{x}) |\tilde{\mathbf{u}}_{\text{turb}}(w, \mathbf{x})|^2 \rangle_{\delta(\mathbf{x})=\delta}, \quad (15)$$

where the environment is specified with the density contrast δ and the mean $\langle \dots \rangle_{\delta(\mathbf{x})=\delta}$ is performed over all the spatial points where the condition $\delta(\mathbf{x}) = \delta$ is satisfied.

For details of the CWT techniques that we have developed, please refer to Wang & He (2021); Wang et al. (2022); Wang & He (2022, 2023, 2024c).

3. RESULTS

We use IllustrisTNG50-1 (hereafter TNG50) simulation data (Pillepich et al. 2018; Nelson et al. 2019a,b; Pillepich et al. 2019) for our work, which is well-suited for studying cosmic fluid turbulence (Wang & He 2024a,b). All the technical details can be found in Section 2. Generally, turbulence

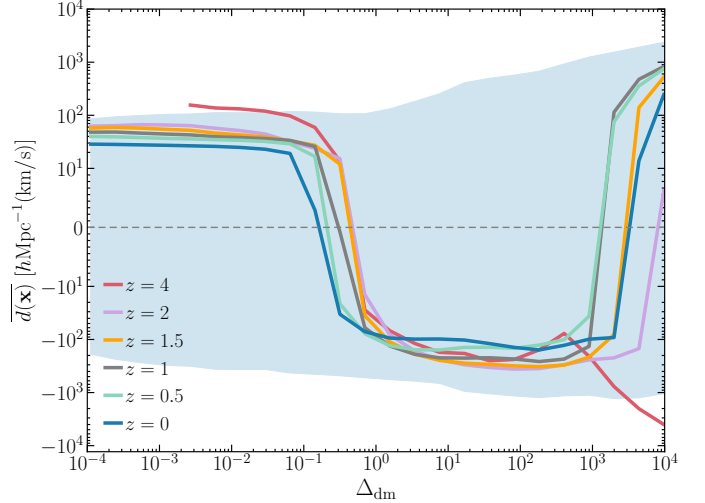


Figure 1. Mean divergence $\overline{d(\mathbf{x})}$ of the baryonic velocity field as a function of dark matter density. For a spatial location \mathbf{x} , there exists the correspondence between the divergence $d(\mathbf{x}) = \nabla \cdot \mathbf{u}(\mathbf{x})$ of baryonic velocity field \mathbf{u} and the dark matter density $\Delta_{\text{dm}}(\mathbf{x}) = \rho_{\text{dm}}(\mathbf{x})/\bar{\rho}_{\text{dm}}$. For a density interval centered at Δ_{dm} , we count all the points within this interval, and in this way, we can calculate the mean value and the standard deviation of $d(\mathbf{x})$. The color band indicates the standard deviations for the values above and below the mean, which are calculated separately. For clarity, only the deviations for $z = 0$ are displayed; the results for other redshifts are similar to those of $z = 0$. Throughout the article, we use an overbar to indicate a statistically averaged quantity.

can exert both dynamical and thermodynamic influences on the cosmic fluid, and we will first discuss the dynamical effects.

In Figure 1, we present the mean divergence $\overline{d(\mathbf{x})}$ of the baryonic velocity field as a function of dark matter density Δ_{dm} . We observe that $\overline{d} > 0$ in the low-density range, indicating that the fluid is statistically diverging or expanding, i.e., there is a net outflow of fluid from the spatial region. Conversely, $\overline{d} < 0$ in the intermediate- and high-density ranges, indicating that the fluid is statistically converging or being compressed, i.e., there is a net inflow of fluid into the region. In the extremely high-density range, which corresponds to small-scale structures such as galaxies, for the highest redshift $z = 4$, there is a rapid decrease in divergence, which may indicate an inflow due to rapid star formation activities. For lower redshifts, the divergences undergo rapid growth, which can be attributed to outflows driven by strong astrophysical processes, such as supernova (SN) feedback or active galactic nucleus (AGN) activities (Magorrian et al. 1998; Silk & Rees 1998; King & Pounds 2015; Harrison et al. 2018; Sharma & Nath 2013; Nelson et al. 2019c; Clavijo-Bohórquez et al. 2024). These outflows increase from $z = 2$ to $z = 1$, nearly remain constant down to $z = 0.5$, and then decrease until the present.

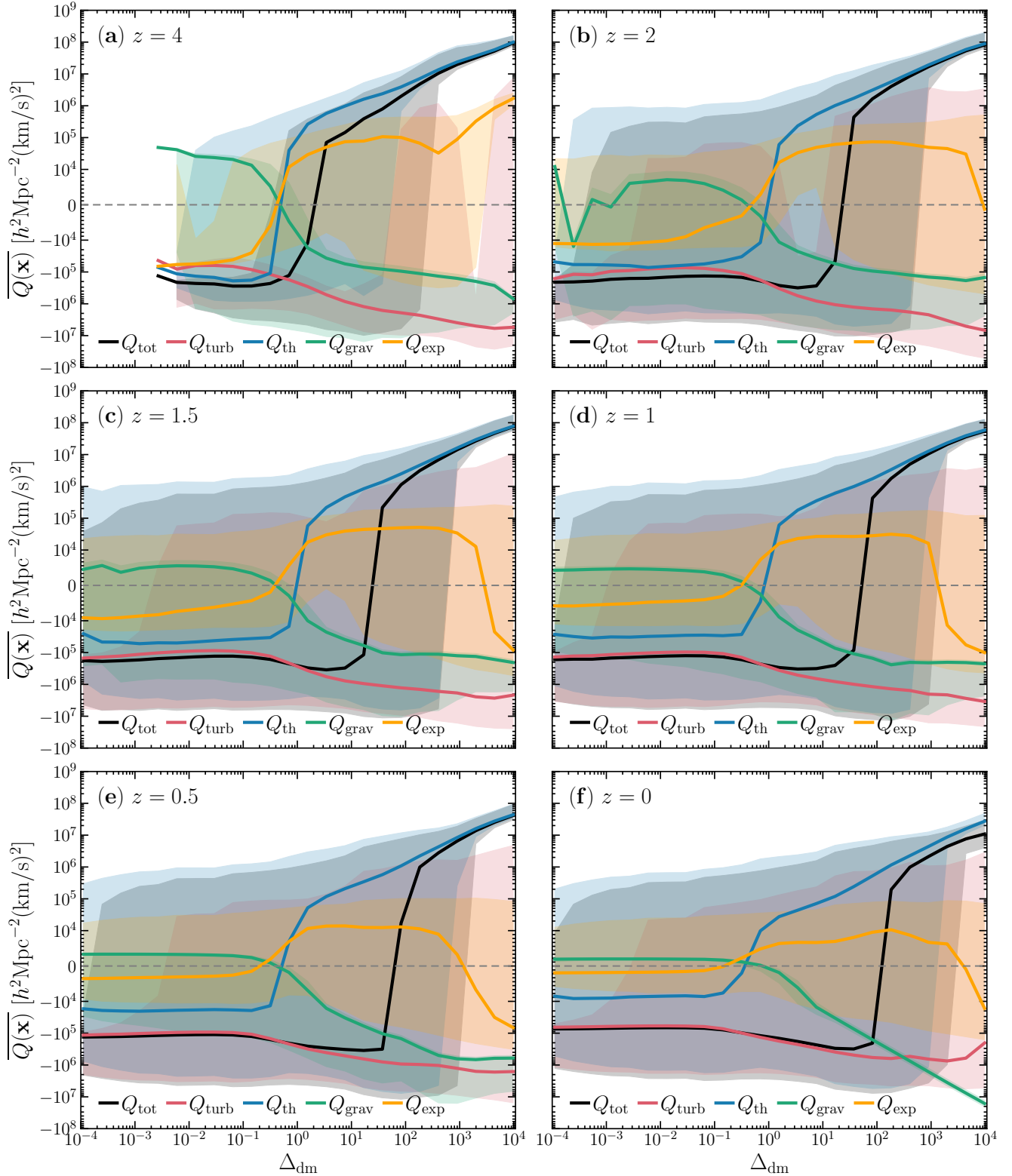


Figure 2. Mean dynamical effects as a function of dark matter density. The mean dynamical effects of turbulence and thermal motion in the cosmic fluid, as well as the gravitational effect, the cosmic expansion effect, and their combined effects, are represented by Q_{turb} , Q_{th} , Q_{grav} , Q_{exp} and Q_{tot} , respectively. Panels (a) to (f) are for $z = 4$ to 0 , respectively. The lines represent the mean values of $Q(\mathbf{x})$, and the color bands indicate the standard deviations for the values above and below the mean, which are calculated separately.

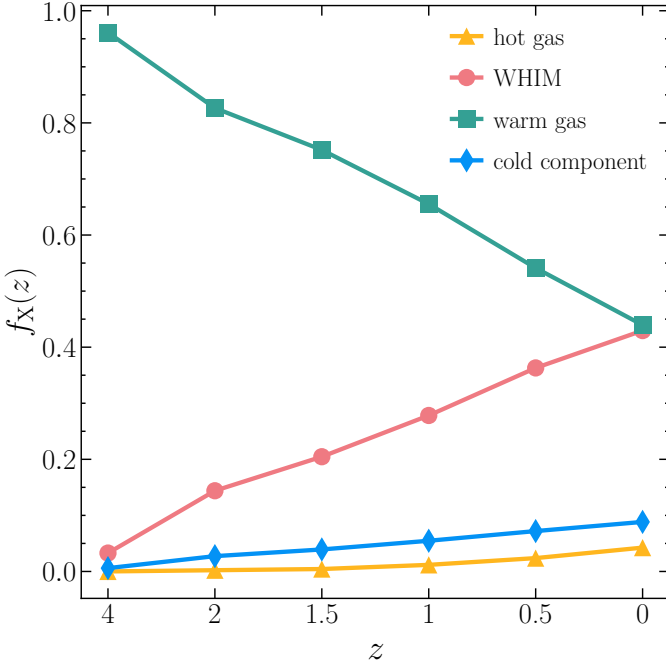


Figure 3. Mass fraction as a function of redshift. The mass fractions of the 4 baryonic components evolve with redshift.

In Figure 2, we present the mean dynamical effects as a function of Δ_{dm} . These dynamical Q -terms are computed using equations (1) and (2). The physical effects of these Q -terms are evident: when $Q > 0$, the corresponding effect drives the spatial region or cosmic structure to expand, whereas when $Q < 0$, it drives the region/structure to collapse. We observe that the cosmic expansion effect \bar{Q}_{exp} simply dampens the flow of the fluid – it suppresses the outflow of gas in both low- and extremely high-density regions (except for the highest redshift $z = 4$), and suppresses the inflow of gas in intermediate- and high-density regions. For all redshifts, the gravitational effect \bar{Q}_{grav} tends to expand the gas in low-density regions while compressing the gas in all other regions. Generally, except in high-density regions at $z = 0$, \bar{Q}_{exp} and \bar{Q}_{grav} are secondary dynamical effects compared to the turbulent effect \bar{Q}_{turb} and the thermal effect \bar{Q}_{th} .

Below, we will specifically analyze the turbulent effect \bar{Q}_{turb} , the thermal effect \bar{Q}_{th} and the total combined effect \bar{Q}_{tot} of the gas. We observe that for all redshifts, $\bar{Q}_{\text{turb}} < 0$ in all regions, and $\bar{Q}_{\text{th}} < 0$ in low-density regions, but $\bar{Q}_{\text{th}} > 0$ in all other regions. In both low- and intermediate-density regions, $\bar{Q}_{\text{tot}} < 0$ and is dominated by \bar{Q}_{turb} . The dynamical effects prevent the outflow of the gas in low-density regions and promote the inflow of the gas in intermediate-density regions, causing the gas to be detained in these regions. As previously addressed in Wang & He (2024b), in high-density regions, the dynamical effects of turbulence and thermal pres-

sure are exactly opposite: $\bar{Q}_{\text{th}} > 0$ while $\bar{Q}_{\text{turb}} < 0$. However, the total combined effect $\bar{Q}_{\text{tot}} > 0$ aligns with the thermal effect \bar{Q}_{th} , thereby suppressing the inflow of the gas. We cannot account for the outflow in the extremely high-density regions, as we have not included AGN or SN feedbacks into the dynamical equation (1).

Notice that \bar{Q}_{turb} actually represents the combined effects of both bulk and turbulent flow. As analyzed in Wang & He (2024b), bulk flow dominates over turbulent flow at high redshifts, while turbulence becomes increasingly dominant as redshift decreases. At $z = 0$, the bulk flow exclusively affects low-density regions, whereas turbulence prevails in all other regions.

In Figure 3, we illustrate how the mass fractions of the 4 baryonic components evolve as a function of redshift. We observe that both the cold component and hot gas gradually increase from near zero at $z = 4$ to 8.8% and 4.3%, respectively, at $z = 0$. However, the most notable change is the significant decrease in the warm gas fraction from 96% to 44%, while the WHIM fraction increases from 3.3% to 43% at the present time. This suggests that there must be some heating mechanism responsible for such a transition. We will address this issue using the cumulative mass fraction, a function of dark matter density Δ_{dm} , which is employed to measure the mass distribution within regions or structures where the density exceeds Δ_{dm} .

Figure 4 displays the cumulative mass fraction F_x for the 4 baryonic components as well as F_{tot} for the total matter as a function of the reverse Δ_{dm} . It is observed that the z -evolution of these F_x is consistent with that shown in Figure 3, and we focus solely on the case at $z = 0$. We note that F_{hot} quickly rises to 3.7% at $\Delta_{\text{dm}} = 200$ and then gradually increases to the saturation fraction of 4.3% towards the lowest-density regions. This suggests that hot gas is predominantly concentrated in virialized structures and slightly extends towards low-density regions. For the cold component, F_{cold} swiftly reaches 8.6% at $\Delta_{\text{dm}} = 10^3$ and remains nearly constant thereafter, indicating that the cold component is entirely confined within galaxies. Regarding the WHIM and warm gas, both F_{WHIM} and F_{warm} increase gradually with decreasing dark matter density, extending to the lowest-density regions with an increasingly gentle growth rate. However, the spatial distribution of the warm gas is more extended than that of the WHIM. Examining the z -evolution of F_{tot} , we find that for $\Delta_{\text{dm}} > 200$, baryonic matter continues to accumulate with time, reaching 28% at $\Delta_{\text{dm}} = 200$ by $z = 0$. This suggests that over 70% of baryons at the present time reside in outer regions where $\Delta_{\text{dm}} < 200$.

In Figure 5, we present the baryon fraction for the total gas of different redshifts. At $z = 4$, we see that most of the baryons reside in intermediate-density regions, with baryon

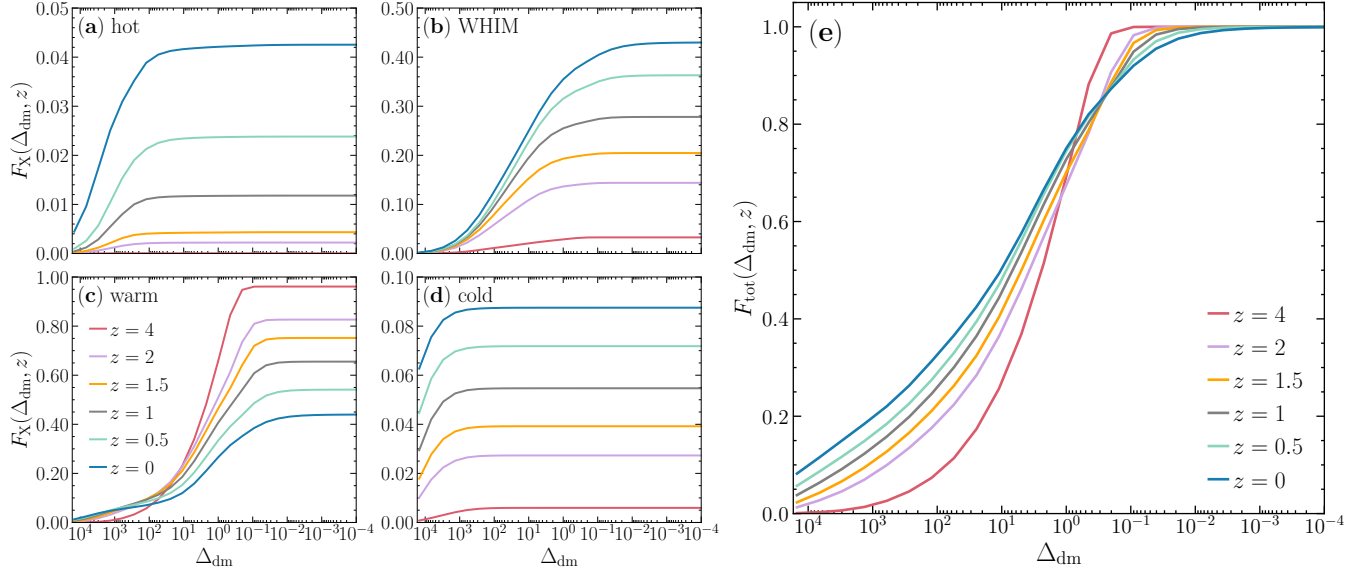


Figure 4. Cumulative mass fraction as a function of dark matter density. The cumulative mass fraction F_x for hot gas (a), WHIM (b), warm gas (c) and cold component (d) are presented, respectively. The total cumulative mass fraction F_{tot} is shown in Panel (e). Both F_x and F_{tot} are functions of dark matter density Δ_{dm} and redshift z . The subscript ‘x’ can be replaced with ‘hot’, ‘WHIM’, ‘warm’ or ‘cold’ as required.

fractions centered around the cosmic mean value of \bar{f}_b . Consistent with the above analysis, as time progresses, dark matter rapidly concentrates and may even form virialized structures, but baryonic matter increasingly decouples from dark matter, leading to a more extended spatial distribution (He et al. 2004). Consequently, baryon fractions are relatively low in high- and extremely high-density regions but are high in low- and intermediate-density regions, as seen in the panels of low redshifts. This accounts for the presence of the ‘high baryon fraction phase’ gas (He et al. 2005).

We now examine the thermodynamic mechanisms underlying the behaviors of baryonic gas. In this study, we calculate the energy densities of turbulence and thermal energy at different redshifts and analyze their z -evolution. This approach allows us to infer the heating and radiative cooling rates of the baryonic fluid. Figure 6 displays the mean thermal energy densities $\bar{\varepsilon}_{\text{th}}$, turbulent energy densities $\bar{\varepsilon}_{\text{turb}}$, and their mean ratios \bar{r} of the baryonic fluid at different redshifts as a function of Δ_{dm} . As illustrated in Figures 6(a) and (b), both $\bar{\varepsilon}_{\text{th}}$ and $\bar{\varepsilon}_{\text{turb}}$ increase with Δ_{dm} , yet their evolution from $z = 1$ to $z = 0$ is extremely weak, indicating that the cosmic fluid is essentially in a state of fully-developed turbulence in this redshift range. The measurements in Figure 6(c) reveal that at low redshifts of $z \leq 1$, the mean ratios \bar{r} are approximately twice as high in both low- and extremely high-density regions. Conversely, in intermediate- and high-density regions, the ratios fall below one, with a minimum value of one-half observed at $\Delta_{\text{dm}} \sim 200$ for $z = 0$. The z -evolution of the ratios is not significant at low redshifts, as the differences in ratios range only between 1 to 2 times between $z = 1$ and $z = 0$.

At $z = 0$, if the dissipation of turbulent and thermal energy is roughly in balance, it is reasonable to expect that the ratio of energy densities, \bar{r} , would be approximately 1. However, as aforementioned, there is a deviation from 1, and the reasons for this deviation are as follows. In low- and extremely high-density regions, $\bar{d} > 0$, and the fluid can be approximated as adiabatically expanding, which leads to a decrease in temperature T and a drop in thermal energy density ε_{th} . Accordingly, we know from equations (9) and (12) that \bar{r} will increase. Conversely, in intermediate- and high-density regions, $\bar{d} < 0$, then the fluid can be approximated as adiabatically compressing, which leads to an increase in T and an increase in thermal energy density ε_{th} , thereby decreasing \bar{r} .

Below, we examine the turbulent energy spectrum of the cosmic fluid. Figure 7 displays the z -evolution of the environment-dependent wavelet energy spectrum of turbulence. We observe that, while these spectra are very similar to each other, there are indeed some differences. Specifically, the amplitudes of the spectra increase with higher environmental density and generally grow as redshift decreases. However, it should be noted that from $z = 1$ to $z = 0$, the shapes and amplitudes of the spectra remain essentially unchanged. This suggests that the injection and dissipation of turbulent energy have essentially reached a balance, indicating once again that the fluid is in a state of fully-developed turbulence within this redshift range. Additionally, within the inertial range where $k > k_{\text{peak}}$, the power index becomes increasingly flat as redshift decreases and environmental density increases. The power index is -1.62 for the case of $\Delta_{\text{dm}} \in [8, \infty)$ at $z = 0$ (see Figure 7(c)), which is close

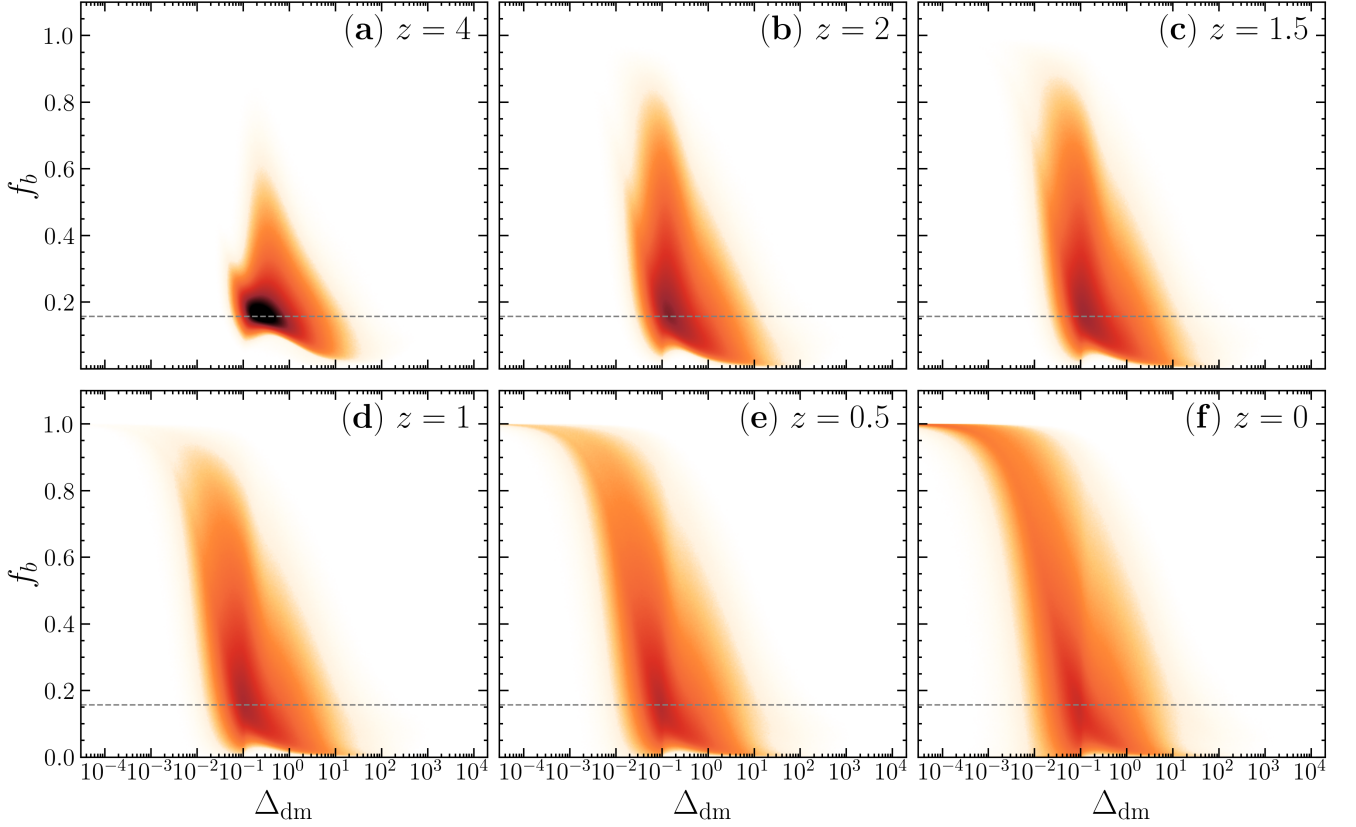


Figure 5. Scatter plot of baryon fraction as a function of dark matter density. Panels (a) to (f) are for $z = 4$ to 0 , respectively. The horizontal dashed line indicates the cosmic mean value of baryon fraction, $\bar{f}_b = 0.1573$.

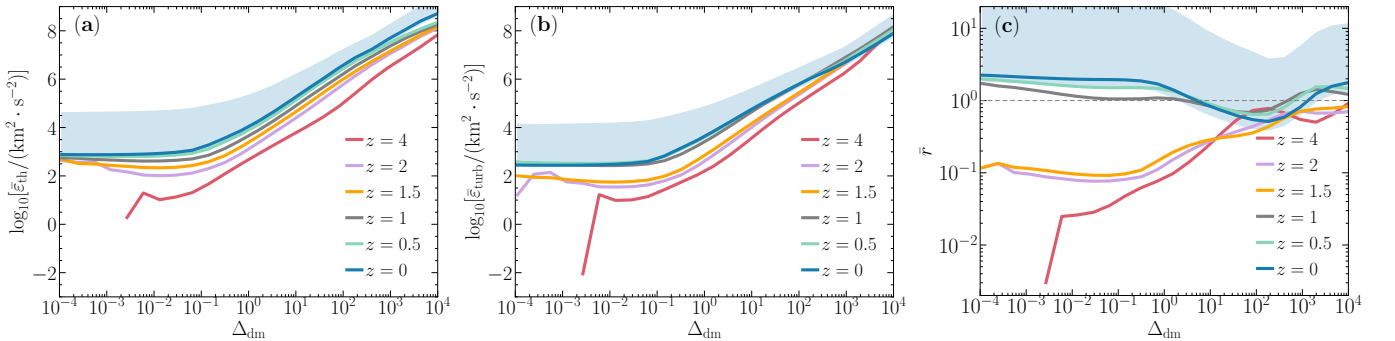


Figure 6. Mean energy densities and energy ratios as a function of dark matter density. Panels (a) and (b) show the mean energy densities of thermal and turbulent energy at different redshifts, respectively. Panel (c) shows the energy ratios of turbulence to thermal energy. The lines represent the mean values, and the color bands indicate the standard deviations of the values above and below the mean, which are calculated separately. For clarity, only the deviations for $z = 0$ are shown; the results for other redshifts are analogous to those of $z = 0$.

to the Kolmogorov index of $-5/3$. As analyzed in Wang & He (2024a), the energy dissipation rate for turbulence with a steeper power index than $-5/3$ is higher than that of Kolmogorov turbulence.

We show the scatter plot of gas temperature versus Δ_{dm} in Figure 8. At $z = 4$, we observe that the majority of baryons are in the form of warm gas. As redshift decreases, an increasing amount of warm gas is heated and transitions into the WHIM, with some even transforming into hot gas. Con-

sequently, the mass fraction of warm gas gradually decreases, while that of the WHIM gradually increases. In the case of $z = 0$, we find that the WHIM is distributed across nearly all regions but is predominantly concentrated in intermediate-density regions. These findings are consistent with the results shown in Figure 4 and Figure 3.

We discuss two previous works that are relevant to the thermodynamic effects of turbulence in cosmic fluids. The first work, utilizing the WIGEON cosmological hydrodynamic

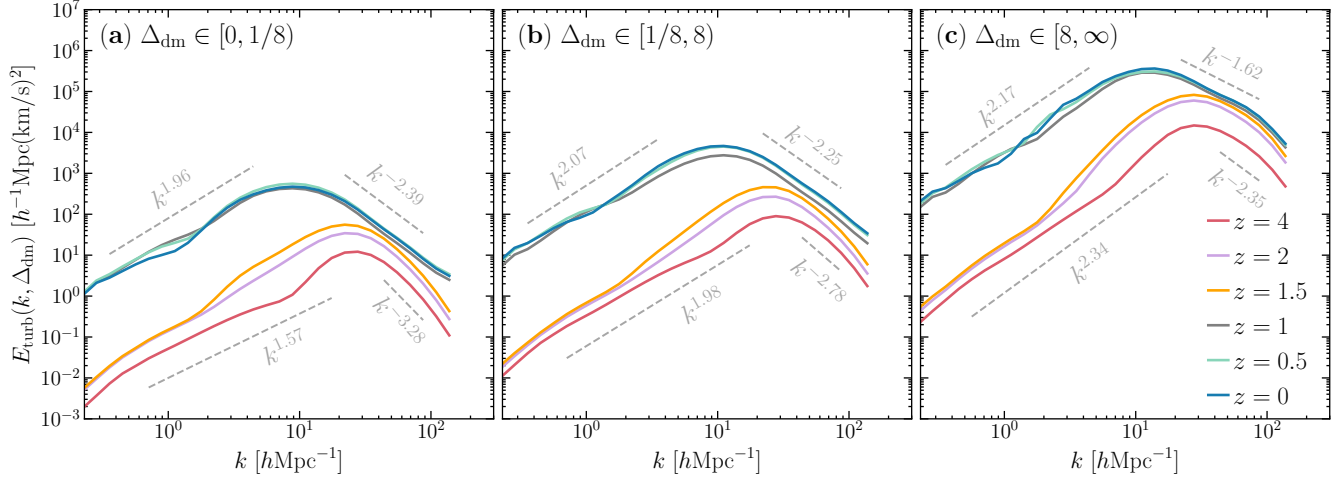


Figure 7. z -evolution of environment-dependent wavelet energy spectra of turbulence. Panels (a), (b) and (c) show the energy spectra of three intervals of dark matter density Δ_{dm} as indicated in the figure. The energy spectra $E_{\text{turb}}(k, \delta)$ are obtained from the env-WPS in equation (15) as $E_{\text{turb}}(k, \delta) = k^2 S_{\text{turb}}(k, \delta)$. The relevant power-law fits for the scale ranges that are smaller and larger than the peak positions k_{peak} are indicated in the figure.

simulations (Feng et al. 2004, Zhang et al. (2006) shows that the cosmic baryonic fluid in the nonlinear regime behaves like Burgers turbulence, which plays a significant role in converting kinetic energy into thermal energy, thereby heating the gas. Moreover, it appears that heating by Burgers turbulence alone is sufficient to account for the basic features of X-ray emission from baryonic gas in the universe. The second work, through an investigation of the turbulent heating rate and radiative cooling rate in the intra-cluster medium (ICM) of the Perseus and Virgo clusters, Zhuravleva et al. (2014) suggests that turbulent heating is sufficient to offset radiative cooling at each radius of the clusters, implying that turbulence is a powerful thermal source to heat the ICM. These findings support the conclusions of our current work.

4. CONCLUSIONS AND DISCUSSIONS

Turbulence in the cosmic baryonic fluid can exert both dynamical and thermodynamic influences on cosmic baryons. For the dynamical aspect of turbulence, we find that in both the low- and intermediate-density regions, the dynamical effects are negative and dominated by turbulence, that is $\overline{Q}_{\text{tot}} \sim \overline{Q}_{\text{turb}} < 0$. These negative dynamical effects suppress outflow in low-density regions but promote inflow in intermediate-density regions, which causes the gas to be detained in these regions. Conversely, in high-density regions, the dynamical effects are positive and dominated by thermal pressure, that is $\overline{Q}_{\text{tot}} \sim \overline{Q}_{\text{th}} > 0$, which will prevent the inflow of the gas. These dynamical effects result in high baryon fractions in low- and intermediate-density regions, but low baryon fractions in high-density regions. Furthermore, the cumulative mass fraction reveals that both the WHIM and warm gas are more extensively distributed in space.

For the thermodynamic aspect of turbulence, turbulent energy is converted into thermal energy in two primary ways. Firstly, turbulent kinetic energy cascades from large-scale to small-scale eddies, dissipating into heat when the scale falls below the Kolmogorov length, which is suitable for Kolmogorov turbulence. Secondly, if the power index of turbulent energy spectra is steeper than the Kolmogorov index, kinetic energy can be directly dissipated into thermal energy via shock heating within the inertial range. Consequently, the energy dissipation rate for turbulence with a power index steeper than $-5/3$ exceeds that of Kolmogorov turbulence (Wang & He 2024a). It can be seen, from $z = 1$ to $z = 0$, that both the mean thermal energy density $\overline{\epsilon}_{\text{th}}$ and the mean turbulent energy density $\overline{\epsilon}_{\text{turb}}$ remain nearly constant, and the shapes and amplitudes of the environment-dependent wavelet energy spectra are essentially unchanged. These findings indicate that the injection and dissipation of turbulent energy have essentially reached a balance, and the cosmic fluid is in a state of fully-developed turbulence within this redshift range.

Due to turbulent heating, we see that as redshift decreases, an increasing amount of warm gas is heated and transitions into the WHIM, and some even into hot gas. Consequently, the mass fraction of warm gas gradually decreases, while that of the WHIM increases. The WHIM is distributed in nearly all regions, with the majority concentrated in intermediate-density regions.

Additionally, a related issue is the overcooling problem (Voit 2005). If the gas cools too much, it could lead to an overabundance of stars and galaxies forming at early times, which is inconsistent with observational data. Thus, feedback from SN and AGN is proposed to resolve the problem. However, as addressed in Silk & Nusser (2010), black holes

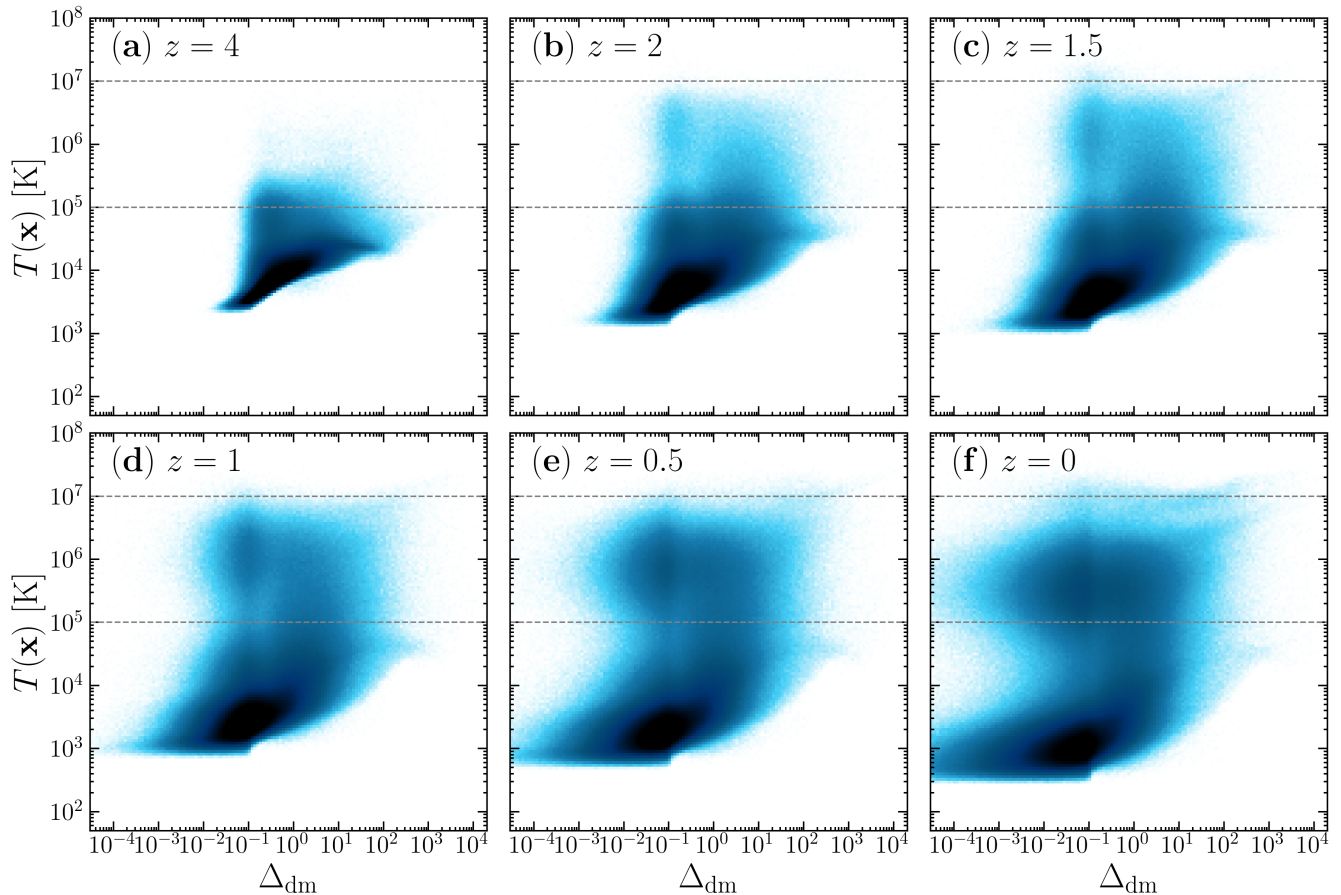


Figure 8. Scatter plot of baryonic temperature as a function of dark matter density. Panels (a) - (f) are for $z = 4$ to 0 , respectively. Gas with $T < 10^5$ K is the warm gas, gas with $T > 10^7$ K is the hot gas, and gas with temperature between these two ranges is the WHIM.

cannot supply sufficient momentum in radiation to expel the gas by pressure alone. We propose that, in addition to SN feedback and AGN activities, turbulent heating should also be a potential heating mechanism to overcome the overcooling problem.

In summary, through dynamical and thermodynamic studies of the cosmic baryonic fluid, we have provided a physical explanation for the missing baryon problem.

ACKNOWLEDGEMENTS

We acknowledge the use of the data from IllustrisTNG simulation for this work. We also acknowledge the support by the National Science Foundation of China (No. 12147217, 12347163), the China Postdoctoral Science Foundation (No. 2024M761110), and the Natural Science Foundation of Jilin Province, China (No. 20180101228JC).

REFERENCES

- Angelinelli, M., Vazza, F., Giocoli, C., et al. 2020, MNRAS, 495, 864, doi: [10.1093/mnras/staa975](https://doi.org/10.1093/mnras/staa975)
- Banerjee, N., & Sharma, P. 2014, MNRAS, 443, 687, doi: [10.1093/mnras/stu1179](https://doi.org/10.1093/mnras/stu1179)
- Bonafede, A., Feretti, L., Murgia, M., et al. 2010, A&A, 513, A30, doi: [10.1051/0004-6361/200913696](https://doi.org/10.1051/0004-6361/200913696)
- Branchini, E., Ursino, E., Corsi, A., et al. 2009, ApJ, 697, 328, doi: [10.1088/0004-637X/697/1/328](https://doi.org/10.1088/0004-637X/697/1/328)
- Bregman, J. N. 2007, ARA&A, 45, 221, doi: [10.1146/annurev.astro.45.051806.110619](https://doi.org/10.1146/annurev.astro.45.051806.110619)
- Brüggen, M., Hoeft, M., & Ruszkowski, M. 2005, ApJ, 628, 153, doi: [10.1086/430732](https://doi.org/10.1086/430732)
- Cassano, R., & Brunetti, G. 2005, MNRAS, 357, 1313, doi: [10.1111/j.1365-2966.2005.08747.x](https://doi.org/10.1111/j.1365-2966.2005.08747.x)
- Cen, R., & Ostriker, J. P. 1999, ApJ, 514, 1, doi: [10.1086/306949](https://doi.org/10.1086/306949)

- Churazov, E., Vikhlinin, A., Zhuravleva, I., et al. 2012, *MNRAS*, 421, 1123, doi: [10.1111/j.1365-2966.2011.20372.x](https://doi.org/10.1111/j.1365-2966.2011.20372.x)
- Clavijo-Bohórquez, W. E., de Gouveia Dal Pino, E. M., & Melioli, C. 2024, *MNRAS*, 535, 1696, doi: [10.1093/mnras/stae487](https://doi.org/10.1093/mnras/stae487)
- Davé, R., Cen, R., Ostriker, J. P., et al. 2001, *ApJ*, 552, 473, doi: [10.1086/320548](https://doi.org/10.1086/320548)
- Dolag, K., Vazza, F., Brunetti, G., & Tormen, G. 2005, *MNRAS*, 364, 753, doi: [10.1111/j.1365-2966.2005.09630.x](https://doi.org/10.1111/j.1365-2966.2005.09630.x)
- Driver, S. 2021, *Nat.Astron.*, 5, 852, doi: [10.1038/s41550-021-01441-w](https://doi.org/10.1038/s41550-021-01441-w)
- Enßlin, T. A., & Vogt, C. 2006, *A&A*, 453, 447, doi: [10.1051/0004-6361:20053518](https://doi.org/10.1051/0004-6361:20053518)
- Evoli, C., & Ferrara, A. 2011, *MNRAS*, 413, 2721, doi: [10.1111/j.1365-2966.2011.18343.x](https://doi.org/10.1111/j.1365-2966.2011.18343.x)
- Fang, T. 2018, *Nature*, 558, 375, doi: [10.1038/d41586-018-05432-2](https://doi.org/10.1038/d41586-018-05432-2)
- Fang, T., Marshall, H. L., Lee, J. C., Davis, D. S., & Canizares, C. R. 2002, *ApJ*, 572, L127, doi: [10.1086/341665](https://doi.org/10.1086/341665)
- Fang, T., Mckee, C. F., Canizares, C. R., & Wolfire, M. 2006, *ApJ*, 644, 174, doi: [10.1086/500310](https://doi.org/10.1086/500310)
- Feng, L.-L., Shu, C.-W., & Zhang, M. 2004, *ApJ*, 612, 1, doi: [10.1086/422513](https://doi.org/10.1086/422513)
- Fukugita, M., Hogan, C. J., & Peebles, P. J. E. 1998, *ApJ*, 503, 518, doi: [10.1086/306025](https://doi.org/10.1086/306025)
- Gaspari, M., Melioli, C., Brighenti, F., & D’Ercole, A. 2011, *MNRAS*, 411, 349, doi: [10.1111/j.1365-2966.2010.17688.x](https://doi.org/10.1111/j.1365-2966.2010.17688.x)
- Harrison, C. M., Costa, T., Tadhunter, C. N., et al. 2018, *Nature Astronomy*, 2, 198, doi: [10.1038/s41550-018-0403-6](https://doi.org/10.1038/s41550-018-0403-6)
- He, P., Feng, L.-L., & Fang, L.-Z. 2004, *ApJ*, 612, 14, doi: [10.1086/422446](https://doi.org/10.1086/422446)
- . 2005, *ApJ*, 623, 601, doi: [10.1086/428708](https://doi.org/10.1086/428708)
- He, P., Liu, J., Feng, L.-L., Shu, C.-W., & Fang, L.-Z. 2006, *PhRvL*, 96, 051302, doi: [10.1103/PhysRevLett.96.051302](https://doi.org/10.1103/PhysRevLett.96.051302)
- Iapichino, L., Federrath, C., & Klessen, R. S. 2017, *MNRAS*, 469, 3641, doi: [10.1093/mnras/stx882](https://doi.org/10.1093/mnras/stx882)
- Khatri, R., & Gaspari, M. 2016, *MNRAS*, 463, 655, doi: [10.1093/mnras/stw2027](https://doi.org/10.1093/mnras/stw2027)
- Kim, B., He, P., Pando, J., Feng, L.-L., & Fang, L.-Z. 2005, *ApJ*, 625, 599, doi: [10.1086/429556](https://doi.org/10.1086/429556)
- King, A., & Pounds, K. 2015, *ARA&A*, 53, 115, doi: [10.1146/annurev-astro-082214-122316](https://doi.org/10.1146/annurev-astro-082214-122316)
- Lau, E. T., Kravtsov, A. V., & Nagai, D. 2009, *ApJ*, 705, 1129, doi: [10.1088/0004-637X/705/2/1129](https://doi.org/10.1088/0004-637X/705/2/1129)
- Macquart, J. P., Prochaska, J. X., McQuinn, M., et al. 2020, *Nature*, 581, 391, doi: [10.1038/s41586-020-2300-2](https://doi.org/10.1038/s41586-020-2300-2)
- Magorrian, J., Tremaine, S., Richstone, D., et al. 1998, *ApJ*, 115, 2285, doi: [10.1086/300353](https://doi.org/10.1086/300353)
- Miniati, F. 2014, *ApJ*, 782, 21, doi: [10.1088/0004-637X/782/1/21](https://doi.org/10.1088/0004-637X/782/1/21)
- Murgia, M., Govoni, F., Feretti, L., et al. 2004, *A&A*, 424, 429, doi: [10.1051/0004-6361:20040191](https://doi.org/10.1051/0004-6361:20040191)
- Nelson, D., Springel, V., Pillepich, A., et al. 2019a, *Computational Astrophysics and Cosmology*, 6, 2, doi: [10.1186/s40668-019-0028-x](https://doi.org/10.1186/s40668-019-0028-x)
- Nelson, D., Pillepich, A., Springel, V., et al. 2019b, *MNRAS*, 490, 3234, doi: [10.1093/mnras/stz2306](https://doi.org/10.1093/mnras/stz2306)
- . 2019c, *MNRAS*, 490, 3234, doi: [10.1093/mnras/stz2306](https://doi.org/10.1093/mnras/stz2306)
- Nevalainen, J., Tempel, E., Ahoranta, J., et al. 2019, *A&A*, 621, A88, doi: [10.1051/0004-6361/201833109](https://doi.org/10.1051/0004-6361/201833109)
- Nicastro, F., Kaastra, J., Krongold, Y., et al. 2018, *Nature*, 558, 406, doi: [10.1038/s41586-018-0204-1](https://doi.org/10.1038/s41586-018-0204-1)
- Norman, M. L., & Bryan, G. L. 1999, in *The Radio Galaxy Messier 87*, ed. H.-J. Röser & K. Meisenheimer, Vol. 530 (Springer-Verlag Berlin Heidelberg), 106
- Pillepich, A., Springel, V., Nelson, D., et al. 2018, *MNRAS*, 473, 4077, doi: [10.1093/mnras/stx2656](https://doi.org/10.1093/mnras/stx2656)
- Pillepich, A., Nelson, D., Springel, V., et al. 2019, *MNRAS*, 490, 3196, doi: [10.1093/mnras/stz2338](https://doi.org/10.1093/mnras/stz2338)
- Porter, D. H., Jones, T. W., & Ryu, D. 2015, *ApJ*, 810, 93, doi: [10.1088/0004-637X/810/2/93](https://doi.org/10.1088/0004-637X/810/2/93)
- Roediger, E., & Brüggén, M. 2007, *MNRAS*, 380, 1399, doi: [10.1111/j.1365-2966.2007.12241.x](https://doi.org/10.1111/j.1365-2966.2007.12241.x)
- Ryu, D., Kang, H., Cho, J., & Das, S. 2008, *Science*, 320, 909, doi: [10.1126/science.1154923](https://doi.org/10.1126/science.1154923)
- Schmidt, W., Byrohl, C., Engels, J. F., Behrens, C., & Niemeyer, J. C. 2017, *MNRAS*, 470, 142, doi: [10.1093/mnras/stx1274](https://doi.org/10.1093/mnras/stx1274)
- Schuecker, P., Finoguenov, A., Miniati, F., Böhringer, H., & Briel, U. G. 2004, *A&A*, 426, 387, doi: [10.1051/0004-6361:20041039](https://doi.org/10.1051/0004-6361:20041039)
- Sharma, M., & Nath, B. B. 2013, *ApJ*, 763, 17, doi: [10.1088/0004-637X/763/1/17](https://doi.org/10.1088/0004-637X/763/1/17)
- Shi, X., & Zhang, C. 2019, *MNRAS*, 487, 1072, doi: [10.1093/mnras/stz1392](https://doi.org/10.1093/mnras/stz1392)
- Silk, J., & Nusser, A. 2010, *ApJ*, 725, 556, doi: [10.1088/0004-637X/725/1/556](https://doi.org/10.1088/0004-637X/725/1/556)
- Silk, J., & Rees, M. J. 1998, *A&A*, 331, L1, doi: [10.48550/arXiv.astro-ph/9801013](https://doi.org/10.48550/arXiv.astro-ph/9801013)
- Subramanian, K., Shukurov, A., & Haugen, N. E. L. 2006, *MNRAS*, 366, 1437, doi: [10.1111/j.1365-2966.2006.09918.x](https://doi.org/10.1111/j.1365-2966.2006.09918.x)
- Vacca, V., Murgia, M., Govoni, F., et al. 2010, *A&A*, 514, A71, doi: [10.1051/0004-6361/200913060](https://doi.org/10.1051/0004-6361/200913060)
- Vazza, F., Brunetti, G., & Gheller, C. 2009, *MNRAS*, 395, 1333, doi: [10.1111/j.1365-2966.2009.14691.x](https://doi.org/10.1111/j.1365-2966.2009.14691.x)
- Vazza, F., Roediger, E., & Brüggén, M. 2012, *A&A*, 544, A103, doi: [10.1051/0004-6361/201118688](https://doi.org/10.1051/0004-6361/201118688)
- Vogt, C., & Enßlin, T. A. 2003, *A&A*, 412, 373, doi: [10.1051/0004-6361:20031434](https://doi.org/10.1051/0004-6361:20031434)
- Voit, G. M. 2005, *Rev. Mod. Phys.*, 77, 207, doi: [10.1103/RevModPhys.77.207](https://doi.org/10.1103/RevModPhys.77.207)
- Walker, S. A., Sanders, J. S., & Fabian, A. C. 2015, *MNRAS*, 453, 3699, doi: [10.1093/mnras/stv1929](https://doi.org/10.1093/mnras/stv1929)

- Wang, Y., & He, P. 2021, *Communications in Theoretical Physics*, 73, 095402, doi: [10.1088/1572-9494/ac10be](https://doi.org/10.1088/1572-9494/ac10be)
- , 2022, *ApJ*, 934, 112, doi: [10.3847/1538-4357/ac7a3d](https://doi.org/10.3847/1538-4357/ac7a3d)
- , 2023, *RAS Techniques and Instruments*, 2, 307, doi: [10.1093/rasti/rzad020](https://doi.org/10.1093/rasti/rzad020)
- , 2024a, *ApJ*, 974, 107, doi: [10.3847/1538-4357/ad6d63](https://doi.org/10.3847/1538-4357/ad6d63)
- , 2024b, *MNRAS*, 534, L14, doi: [10.1093/mnras/lsae073](https://doi.org/10.1093/mnras/lsae073)
- , 2024c, *MNRAS*, 528, 3797, doi: [10.1093/mnras/stae229](https://doi.org/10.1093/mnras/stae229)
- Wang, Y., Yang, H.-Y., & He, P. 2022, *ApJ*, 934, 77, doi: [10.3847/1538-4357/ac752c](https://doi.org/10.3847/1538-4357/ac752c)
- Yang, H.-Y., He, P., Zhu, W., & Feng, L.-L. 2020, *MNRAS*, 498, 4411, doi: [10.1093/mnras/staa2666](https://doi.org/10.1093/mnras/staa2666)
- Yang, H.-Y., Wang, Y., He, P., Zhu, W., & Feng, L.-L. 2022, *MNRAS*, 509, 1036, doi: [10.1093/mnras/stab3062](https://doi.org/10.1093/mnras/stab3062)
- Zhang, T.-J., Liu, J., Feng, L.-L., He, P., & Fang, L.-Z. 2006, *ApJ*, 642, 625, doi: [10.1086/501120](https://doi.org/10.1086/501120)
- Zhu, W., Feng, L.-L., & Fang, L.-Z. 2010, *ApJ*, 712, 1, doi: [10.1088/0004-637X/712/1/1](https://doi.org/10.1088/0004-637X/712/1/1)
- , 2011, *MNRAS*, 415, 1093, doi: [10.1111/j.1365-2966.2011.18640.x](https://doi.org/10.1111/j.1365-2966.2011.18640.x)
- Zhu, W., Feng, L.-L., Xia, Y., et al. 2013, *ApJ*, 777, 48, doi: [10.1088/0004-637X/777/1/48](https://doi.org/10.1088/0004-637X/777/1/48)
- Zhuravleva, I., Churazov, E., Schekochihin, A. A., et al. 2014, *Nature*, 515, 85, doi: [10.1038/nature13830](https://doi.org/10.1038/nature13830)